Matching dynamically varying forces with multi-motor-unit muscle models: A simulation study

Tiina Murtola[1*], Christopher Richards[1]

1 Department of Comparative Biomedical Sciences, Royal Veterinary College, London, UK

* tmurtola@rvc.ac.uk

Abstract

Human muscles exhibit great versatility, generating forces needed for highly athletic but also fine motor tasks under a variety of contraction conditions. While muscle models used in musculoskeletal modelling can exhibit a similar range of versatility, they often lack a realistic structure with multiple motor units (MUs) and rate-coded control. To investigate how these features affect a muscle's ability to generate desired force profiles, we have carried out simulations with nine alternative MU pool models for two different cases: 1) a tibialis anterior muscle generating forces matching an isometric trapezoidal force profile, and 2) a generic shoulder muscle matching force profiles from simulated reaching movements while undergoing predetermined length changes. The results suggest that the characteristics of MU pools can impact the pools' ability to match a given force profile, and that the slowly varying forces of isometric trapezoidal tasks and the relatively fast-changing forces during non-isometric reaching favour different MU pool structures. However, the differences in the performance of different MU pool types are relatively small when considered across all tasks. Furthermore, relatively good force matching results could be obtained with feedforward control utilising a simple mapping from the desired force to a common input signal to all MUs, without a need for feedback corrections. While all MU pool models performed well in the specific conditions tested, our investigation highlights the need to consider the functional characteristics of MU pools. From the perspective of musculoskeletal modelling, rate-coded multi-MU muscles must accomplish a diverse set of dynamic tasks requiring larger force ranges or repeated rapid changes in force. As the range of tasks becomes more realistic, we would expect the properties and construction of MU pools to become increasingly important to achieve good performance.

Author summary

Human muscles are versatile, generating forces needed for highly athletic but also fine motor tasks. Similar versatility is desirable in musculoskeletal modelling, which is used to study human movement under a variety of health conditions. The muscles used in such models are often simplified compared to real muscles, consisting of single rather than multiple motor units (MUs), and controlled with a continuous input rather than spike-like impulses. In this work, we have used computer simulations to investigate how including these realistic muscle features affects a muscle's ability to produce the forces needed for different tasks. We observed that different ways to recruit the MUs and determine the frequency of input spikes have relatively little impact on how well the

muscle can match desired forces both during long sustained contractions and dynamic reaching movements. However, tasks that require a large force range or repeated rapid changes in force can be challenging for MU pools. Hence, our results emphasise that representation of MU pools in musculoskeletal modelling should be considered from the perspective of functionality if the modelled muscles need to be as versatile as real muscles.

Introduction

Vertebrate muscle is known for its mechanical versatility allowing it to perform athletic tasks of high speed, power, and endurance, but also tasks requiring fine motor control and finesse. How this versatility is achieved *in vivo* is not fully understood, but muscles are known to consist of multiple motor units (MUs), each comprising of a motor neuron and the muscle fibres it innervates, and these MUs are recruited to contribute to force generation in a manner depending on task demands [1]. Recent studies have utilised high-density surface electromyography to study recruitment of multiple MUs in slow [2, 3] and explosive [4] contractions in humans, but much of our current understanding of recruitment phenomena remains based on a limited selection of muscles, a small fraction of the MUs in the muscle studied, and isometric tasks. The challenges of studying MU recruitment *in vivo* across the full range of daily motor tasks make it difficult to infer what the functional consequences of specific recruitment strategies are.

Musculoskeletal (MSK) models are used widely to understand human movement and its control across different ages and health conditions (e.g. [5, 6]), and they have potential to unravel links between MU recruitment strategies and the resulting movements. However, the muscles in MSK models are generally represented using a single actuator for each direction of action and controlled using a continuous, amplitude-coded excitation or activation signal (e.g. [7–9]). Such simplifications neglect both the multi-MU structure of real muscles and the physiological recruitment mechanism, which relies on frequency coding of action potentials, rather than amplitude-coded control. The omission of these features not only limits the research questions that can be answered using MSK models, but also leaves the functional consequences of multi-MU properties and rate coding largely unexplored.

Although multi-MU muscles are rarely used in MSK modelling, several models for MU pools (i.e. the population of MUs comprising a muscle) have been proposed. Most MU pool models utilise some aspects of the model by Fuglevand et al. [10], which defines MU characteristics and recruitment processes phenomenologically using explicit mathematical functions. This model, and its subsequent modifications, have been used to study phenomena such as onion-skin firing patterns [11], variability in force production [12, 13], time-dependent changes and fatigue [14–16], and contraction energetics [17]. The common features of MU pool models following the approach by Fuglevand et al. [10] include threshold-based recruitment according to the size principle [18]. Additionally, these models require an explicit relationship between the input driving MU recruitment and the output firing rate, which can vary from simple linear [10] to piece-wise linear [13] to mixed linear-exponential [19]. An alternative approach to model MUs uses leaky integrate-and-fire models, where an excitation impulse is triggered when the motor neuron membrane voltage reaches a threshold [3]. As a consequence, MU firing rate in these models is an emergent characteristic, rather than explicitly modelled. Leaky integrate-and-fire models still rely on thresholding and the size principle, however, limiting their usability in cases where more complex recruitment patterns are known to occur (see [1]). While alternative recruitment strategies, for example matching the mechanical task demand with MU properties [20],

have been proposed, it is not clear how they would be implemented in pools with up to several hundred MUs without off-line optimisation.

Integrating existing MU pool models into MSK models suffers from two interlinked challenges. First, MU pool models have mostly been tested with isometric tasks requiring constant or slowly varying force production, such as constant excitation [10], sustained contraction [14], trapezoidal force production (i.e. ramp up - hold - ramp down) [3], and step-wise force-level increase tasks [19]. Although MU pool models have been combined with tendon dynamics and Hill-type force-velocity-length (FVL) characteristics [13, 17], the long, constant excitation [13] or target force [17] conditions studied result in the MUs operating isometrically for most of the task. However, daily movements require a much wider range of contraction conditions, including notable changes in muscle length and speed during contraction as well as changes in force production that can occur orders of magnitude faster than in tasks previously studied. Second, the practicalities of controlling MU pools are largely unexplored. Although MU pool models with feedback control have been able match constant reference force levels [14, 15, 17, 19, 21] and replicate overshoot features commonly produced by humans [17], the focus has remained on long, sustained force production tasks or intermittent contractions at constant force, with little attention given to the transient behaviour before the system reaches steady state. However, the time scale of many daily movements means that muscle contraction may not be steady-state during the majority of the movement; hence, control approaches accounting solely for the steady-state characteristics of MU pools are not guaranteed to work.

In the present work, we investigate whether the differences in the structure and properties of various MU pool models affect their ability to generate a desired force profile precisely, and to what extent any differences observed are task dependent. To answer these questions, we use computational modelling to compare different MU pool models in two cases: (i) a tibialis anterior (TA) muscle required to match isometric trapezoidal forces, which can be compared with experimental data [2], and (ii) a generic (horizontal) flexor of the shoulder (SF) required to match the forces from simulated reaching movements [22], capturing realistic time scales and non-isometric muscle conditions for MSK modelling. Rather than embedding the multi-MU muscles in MSK models, where the nonlinear system dynamics would impose additional challenges on comparisons, we investigate the MU pools' ability to match force profiles in time-based simulations (i.e. not as curve fitting exercise) while undergoing pre-determined length changes. With an eye towards eventual integration of MU pool models with MSK models, we develop and test a feedforward control strategy of MU pool force production to reduce the need for potentially instability-inducing feedback in MSK models. While the present work is technically motivated, answering these questions can also shed light on the functional role of the large range of MU pool structures observed in human muscles (see [23]).

Models

For the present investigation, muscle force production is assumed to take place under feedforward configuration (Fig 1), where the recruitment and rate coding of N parallel MUs is driven by the desired force and FVL trajectory. The FVL trajectory is a single gain signal that combines the muscle's length and contraction speed state and the way in which that state affects the muscle's force generating capacity. The resulting excitation impulse trains trigger the activation dynamics of each MU, leading to a total muscle force as a sum of the contraction forces of the N MUs. In the present work, we compare nine different MU pool models, which differ in terms of their control and recruitment strategies, whereas the muscle fibres in each pool convert firing rates to

force in an identical manner, as detailed below.

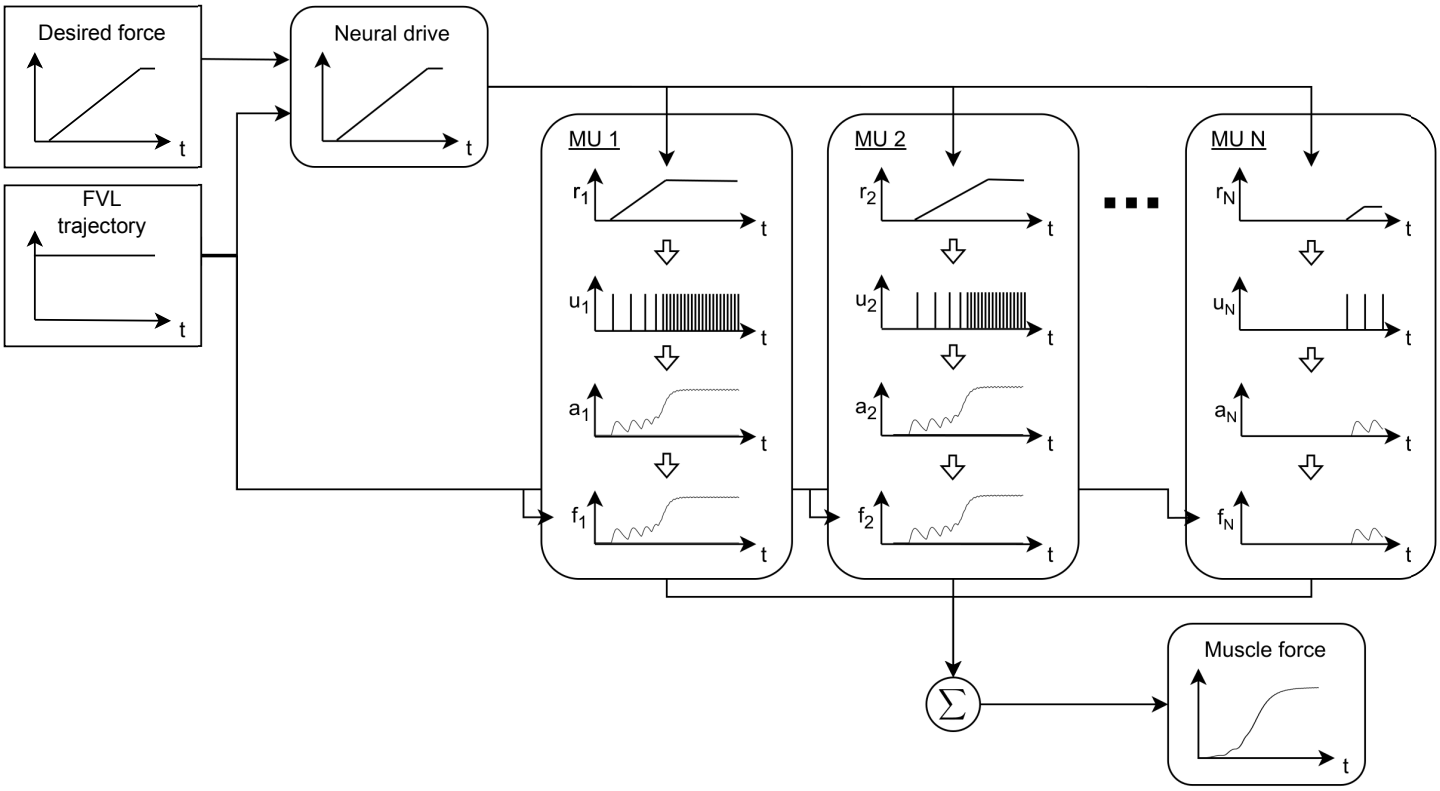

Fig 1. A schematic illustration of force generation in the multi-motor-unit muscle models. Time-based desired force and force-velocity-length (FVL) signals are used to compute neural drive, which governs recruitment, rate coding, and force generation in N parallel motor units (MU).

Motor unit force production model

The total muscle force $F_M(t)$ at time t produced by a pool of MUs, regardless of the pool model, is

$$F_M(t) = \sum_{i=1}^{N} f_i(t). \tag{1}$$

The force $f_i(t)$ produced by the ith MU depends on the length $l = l(t)$ and contraction speed $v = \dot{l}$ of the muscle as well as the activation state of the MU,

$$f_i(t) = f_{max,i} g(l, v) \bar{a}_i(t), \tag{2}$$

where $f_{max,i}$ is the isometric strength of MU i, $i = 1, ..., N$, $g(l, v)$ captures the FVL relationship of the MU, and $\bar{a}_i(t)$ is the normalised activation state of the MU $\bar{a}_i(t) = a_i(u_i(t), t)/a_{max,i} \in [0, 1]$. The unnormalised activation state $a_i(u_i(t), t))$ follows third order activation dynamics [24] driven by an excitation impulse train $u_i(t)$ with instantaneous firing rate $r_i(t) \in [r_{min,i}, r_{max,i}]$, and $a_{max,i}$ corresponds to the unnormalised tetanic activation level when the firing rate is $r_{max,i}$.

For the purposes of the present work, the FVL properties are condensed into a time-dependent trajectory $g(l, v) = g(t)$, which is identical for all MUs. This corresponds to assuming that all MUs have identical normalised length and contraction

speed trajectories, and that their FVL functions are also the same and match the properties underlying the FVL trajectory data in tasks (see below).

The excitation impulse train $u_i(t)$ is constructed from the instantaneous firing rate $r_i(t)$ by identifying the first instants when the time since last impulse exceeds the desired inter-impulse period $1/r_i(t)$. The time $t_{i,k}$ of impulse $k = 1, ...$ for MU i is determined by

$$\min t \in [t_{i,k-1}, T] \quad \text{such that} \quad t \geq t_{i,k-1} + 1/r_i(t) - C_{i,k-1}, \tag{3}$$

where T is the duration of the simulation, and $C_{i,k} = t_{i,k} - t_{i,k-1} - 1/r_i(t_{i,k})$, $k > 1$, $C_{i,1} = 0$, is a corrective term accounting for the error introduced by discrete time, i.e. the fact that the equality in Eq (3) can only hold for a limited set of r_i values during simulations. The computation is initialised with a virtual impulse at $t_{i,0} = -\infty$, which is discarded once the first impulse in the simulation time window $[0, T]$ has been fired. The excitation impulse train is then

$$u_i(t) = \sum_{k=1}^{n_i} p(t - t_{i,k}), \quad \text{where} \tag{4}$$

$$p(t) = \begin{cases} 1 & \text{for } t = 0, \\ 0 & \text{otherwise,} \end{cases} \tag{5}$$

and n_i is the number of impulses for MU i during the simulation time window.

The index $i = 1, .., N$ orders the MUs by size from smallest to largest, with isometric strengths, following [10],

$$f_{max,i} = \frac{R_f^{(i-1)/(N-1)}}{\sum_{i=1}^{N} R_f^{(i-1)/(N-1)}} F_{max}, \tag{6}$$

where $R_f = f_{max,N}/f_{max,1}$ is the range of MU strengths and F_{max} is the isometric strength of the entire muscle. Note that the indexing $(i-1)/(N-1)$ is used to define MU characteristics for ease of parameter interpretation. Given that N is large, the difference compared to the indexing i/N used in the original MU pool [10] is negligible.

Recruitment strategy

Recruitment strategy describes how the firing rate of each MU changes with the desired muscle force $F_d(t)$. It is assumed to comprise of three components: i) a mapping from $F_d(t)$ to neural drive $I(t)$, which acts as the common input driving firing rates for all MUs, ii) a threshold function, which determines the recruitment thresholds δ_i for the MU pool such that the firing rate of MU i is nonzero only when $I(t) \geq \delta_i$, and iii) a rate function, which describes how the firing rate r_i of each MU changes as $I(t)$ increases beyond δ_i. These components are unique for each MU pool model, as detailed below.

Neural drive computation

Ideally, to achieve perfect force matching, the mapping $F_d(t) \longrightarrow I(t)$ should be the inverse of the mapping $I(t) \longrightarrow F_M(t)$. However, given the complex dynamics of MU pools, $F_M(I(t))$ can only be obtained through simulations. This rules out direct curve-fitting of $F_M(t)$ to $F_d(t)$, and it also makes obtaining the inverse $I(F_M(t))$ for a functionally relevant range of operation unfeasible without relying on computationally heavy approaches such as neural networks.

Instead, a simple mapping is constructed using a FVL-normalised desired force and a constant baseline muscle tone with a delay τ between the input and output. The resulting mapping

$$I(t) = \alpha_0 + \alpha_1 \left(\frac{F_d(t+\tau)}{g(t+\tau)} \right)^{\beta} \tag{7}$$

has three parameters, α_0, α_1, and β, in addition to the delay parameter. Given the role of the neural mapping in inverting the MU pool dynamics, the mapping parameters are assumed to depend on the MU pool but to be common for all tasks the MU pool performs. The parameter values are obtained through optimisation using a set of elementary tasks (see below) by seeking the parameters that minimise sum of average square errors

$$\min_{\alpha_0,\alpha_1,\beta,\tau} \sum_k \frac{1}{T} \int_0^T (F_{d,k}(t) - F_M(I(t)))^2 dt, \tag{8}$$

where k is the index for the elementary tasks.

Threshold functions

The MU pool models considered in the present study can be divided into three types based on their recruitment threshold scheme. The first two schemes also define recruitment bandwidths Δ_i for the MUs, that is, the range of neural drive values over which the MU force increases from minimum to maximum.

1. Exponentially assigned recruitment thresholds inspired by [10] with a constant recruitment bandwidth

$$\delta_i = a_1 R_d^{(i-1)/(N-1)} \quad \text{and} \quad \Delta_i = F_{max} - a_1 R_d, \tag{9}$$

   defined by the range of recruitment thresholds $R_d = \delta_N/\delta_1$ and the parameter a_1 which corresponds to the recruitment threshold for the first MU, $a_1 = \delta_1$.

2. Strength-matched recruitment thresholds with constant recruitment band overlap

$$\delta_1 = b_1, \quad \delta_i = \delta_{i-1} + \Delta_{i-1}(1 - b_2), \text{ for } i = 2, ..., N, \quad \text{and} \quad \Delta_i = f_{max,i}, \tag{10}$$

   where b_2 is the overlap, that is, the proportion of Δ_{i-1} where the forces produced by MUs $i-1$ and i are simultaneously increased through rate coding. This threshold scheme is included as a "linearised" version of the above exponential scheme, rather than as a realistic representation of human MU pools. That is, when combined with a linear rate function, the steady-state tetanic force output from MU pools of this type increases roughly linearly with neural drive, which is not true for the other threshold schemes.

3. Mixed linear-exponential recruitment thresholds inspired by [3]

$$\delta_i = c_1 R_c^{((i-1)/(N-1))^{c_3}} + c_2 \frac{i-1}{N-1}, \tag{11}$$

   where $c_1 = \delta_1$, and the parameters R_c, c_2 and c_3 control the shape of function.

Rate functions

Rather than simulating firing rates by modelling realistic membrane dynamics (requiring hundreds of differential equations for a MU pool), for simplicity, we assume that the outcome of this process can be described using explicit rate functions. The simplest,

commonly used rate functions (e.g. [10, 13]) are linear, increasing from minimum firing rate $r_{min,i}$ to maximum firing rate $r_{max,i}$ over the recruitment bandwidth, that is

$$r_i(I) = \begin{cases} 0 & \text{for } I < \delta_i, \\ r_{min,i} + \frac{r_{max,i} - r_{min,i}}{\Delta_i}(I - \delta_i) & \text{for } \delta_i \leq I < \delta_i + \Delta_i, \\ r_{max,i} & \text{otherwise.} \end{cases} \tag{12}$$

Although this rate function does not capture some known effects, such as the tendency for a steeper initial slope [13, 19], it represents the gross firing rate behaviour with minimal parameters.

Alternatively, rate functions can be derived from more complex motor neuron models, such as a single-compartment leaky integrate-and-fire, which produces a logarithmic relationship between the steady-state firing rate and membrane current [3]. Adapting this approach to utilise neural drive $I(t)$, the rate function is

$$r_i(I) = \begin{cases} 0 & \text{for } I \leq \delta_i \\ \left(\frac{1}{r_{max,i}} - \frac{d_1 R_r^{(i/N)^{d_2}}}{\delta_i} \ln(1 - \delta_i/I)\right)^{-1} & \text{otherwise,} \end{cases} \tag{13}$$

where d_1, d_2, and R_r are parameters and ln() is the natural logarithm.

The minimum firing rate $r_{min,i}$ in the linear rate function is assumed to be zero for easy comparison with the logarithmic rate function. While this assumption does not match known MU behaviour at the recruitment threshold (e.g. [13]), the difference is only notable if the neural drive is maintained at a MU's recruitment threshold for long enough to evoke multiple excitation spikes, which is only true for a few MUs in a pool even during long, sustained contractions.

Multiple different ways to characterise the maximum firing rate $r_{max,i}$ have been proposed (e.g. [10, 13, 19]), to account for the variability in experimental data [23] while explaining phenomena such as 'onion-skin' recruitment, where later recruited MUs reach lower firing rates than earlier recruited ones. For the present work, the MU pools are constructed using three r_{max} schemes: the same r_{max} for all MUs, $r_{max,i}$ decreasing linearly with i, and $r_{max,i}$ decreasing exponentially with i.

Motor unit pool parameters

The threshold and rate functions above are combined to obtain three basic types of MU pools (Table 1): exponential-linear (exponential threshold function, linear rate function), matched-linear (strength matched threshold function, linear rate function) and mixed-logarithmic (mixed linear-exponential threshold function, logarithmic rate function). Each MU pool type is combined with the three schemes for maximum firing rates (constant, linear decrease with i, exponential decrease with i), for a total of nine MU pools (Fig 2). The common parameters of these nine MU pools (N, F_{max}, $r_{max,1}$, R_f, δ_1, δ_N, and activation dynamics characterised by time-to-peak and half-relaxation time) are adjusted to represent the two muscles studied, TA and SF (Table 2). For the TA, the MU pools are parameterised to represent the entire muscle. For the SF, however, the MU pools only represent the $N = 200$ smallest MUs whose total strength adds up to $F_{max} = 200$ N, rather than a larger pool representing the entire muscle. This was done because the tasks for the SF only require peak forces less than 40 N (see below), resulting in the muscle's larger, high-threshold MUs never being recruited. The R_f and δ_N values for the SF are set to reflect this partial pool architecture.

To facilitate easy comparison, δ_1 and δ_N are the same for all schemes representing a muscle, and when δ_N is changed to represent TA/SF, it is done via adjustment of a single parameter in each threshold function (Table 1). Based on the muscle specific

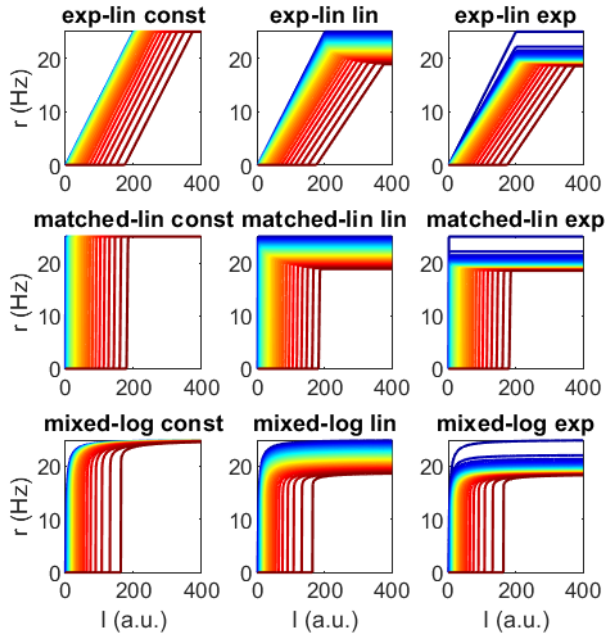

Fig 2. Firing rate functions for the nine MU pool models of TA. Firing rates (r) vs. neural drive (I) for the MUs in pools representing the TA for the different recruitment schemes. The line color varies from dark blue for the first MU to dark red for the last MU. Only every 10th of the 400 MUs are shown.

parameters (Table 2), the threshold function parameters are: $R_d = 400$ for TA and $R_d = 380$ for SF, $b_2 \approx 0.496$ for TA and $b_2 \approx 0.041$ for SF, $c_2 = 29.195$ and $c_3 = 1.833$ for both muscles based on [3], and $R_c \approx 341.6$ for TA and $R_c \approx 321.6$ for SF.

As mentioned above, $r_{min,i} = 0$ for all i. $r_{max,1}$ is set to 25 Hz for TA based on [2,3] to ensure comparability with reference data and to 50 Hz for SF to account for existing data on deltoid during slowly varying contractions [25] and the general observation that rapid contractions can elicit significantly higher firing rates (including double discharges) than slower ones [26]. The parameters for the logarithmic rate function are adapted from [3] to d_1 =0.1, d_2 =1.47, and R_r=2.4. The three r_{max} schemes are parameterised as follows: $r_{max,i} = r_{max,1}$ for $i = 2, ..., N$ for the constant scheme, $r_{max,i} = r_{max,1}(1 - 0.25(i-1)/(N-1))$ for the linear scheme, and $r_{max,i} = r_{max,1} i^{-0.05}$ for the exponential scheme.

Simulations

Tasks

Each task for the simulations is defined as a pair of desired force $F_d(t)$ and FVL trajectory $g(t)$ for time $t \in [0, T]$. Optimisation of the parameters of the neural drive (Eq 7) is done using a set of scaled, artificially constructed elementary tasks. The performance of the MU pool models is then evaluated using tasks based on either experimental or musculoskeletal simulation data.

The task sets for optimisation are constructed using three elementary tasks (Fig 3A): an isometric contraction, and concentric and eccentric contractions where the muscle length follows the minimum-jerk trajectory [27]. In all of these tasks, the target force profile is parabolic, and it occurs during the first half of the movement for the

Table 1. Motor unit pool models: combinations of threshold and rate functions, correspondence between threshold function parameters and first and last thresholds, maximum firing rate schemes, and the abbreviations used in figures.

Threshold/rate func.	δ_1	δ_N	r_{max}	Model abbr.
Exponential/linear	$\delta_1 = a_1$	$\delta_N = R_d\delta_1,\ R_d > 0$	Constant	exp-lin const
			Linear decrease	exp-lin lin
			Exponential decrease	exp-lin exp
Strength matched/linear	$\delta_1 = b_1$	$\delta_N = \delta_1 + (1 - b_2)(F_{max} - f_{max,N})$, $b_2 \in [0, 1]$	Constant	matched-lin const
			Linear decrease	matched-lin lin
			Exponential decrease	matched-lin exp
Mixed/logarithmic	$\delta_1 = c_1$	$\delta_N = c_1 R_c + c_2$	Constant	mixed-log const
			Linear decrease	mixed-log lin
			Exponential decrease	mixed-log exp

Table 2. MU pool characteristics for tibialis anterior and a generic shoulder flexor

Parameter	Tibialis anterior (TA)	Shoulder flexor (SF)
N	400	200
F_{max} (N)	400	200
$r_{max,1}$ (Hz)	25	50
Time-to-peak (ms)	60	70
Half-relaxation time (ms)	70	80
R_f	100	10
δ_1	0.5	0.5
δ_N	$0.5F_{max}$	$0.95F_{max}$

concentric and isometric tasks and during the second half for the eccentric task. The amplitude of the target force is scaled to match the range of forces required during test tasks (see below). This range is achieved using two levels of force amplitude for each muscle, $0.3F_{max}$ and $0.5F_{max}$ for the TA and $0.05F_{max}$ and $0.2F_{max}$ for the SF (Nb. Fig 3A shows the normalised force target before scaling), resulting in a total of six tasks used to optimise the neural drive parameters for each muscle. The duration of all of the tasks is 2 sec, with target force production occurring over 1 sec. All contractions start at optimal muscle length and the change in muscle length is ±20% for the concentric/eccentric tasks. FVL gains are computed from length and contraction speed using the functions in [22], matching the muscle properties used in simulations of test tasks for the SF.

Once the parameters for the neural drive mapping for each MU pool have been obtained, the ability of the MU pools to match functional force profiles is tested. The test tasks for the MU pools representing the TA are slow isometric trapezoidal force profiles with plateaus at 30% and 50% F_{max} matching the experimental conditions of data from [2] (Fig 3B). For the SF, the test tasks are four simulated force profiles with matched FVL trajectories produced by a MSK model of the human arm [22], representing a group of reaching movements where the SF functions as an agonist (Fig 3C).

Matching errors

To quantify the ability of the MU pool models to match desired force profiles, three errors are computed. Each error emphasises a different aspect of the goodness of the match, and they reflect the functionally different contexts in which force production

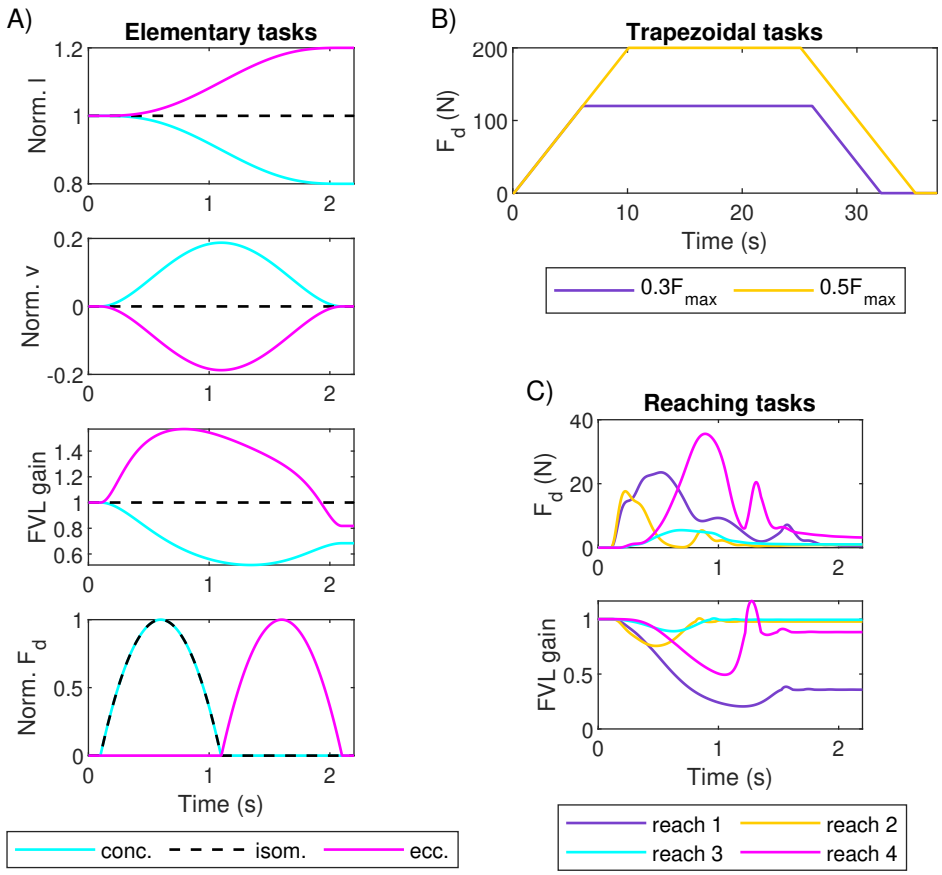

Fig 3. Force matching tasks. (A) Elementary concentric, isometric and eccentric tasks used to optimise neural drive. From the top, panels show normalised muscle length, normalised contraction speed, the resulting FVL gain, and normalised desired force. (B) Trapezoidal tasks with two different force amplitudes. Only desired force is shown as the tasks are isometric. (C) Four reaching tasks with desired forces and FVL gains

tasks could occur. First, the root-mean-square error

$$e_{rms} = \sqrt{\frac{1}{T}\int_0^T \left(F_M(t) - F_d(t)\right)^2 dt} \tag{14}$$

reflects the average match between target and muscle force during each task, and it serves as an overall measure of success. Second, the maximum absolute error normalised with the peak force amplitude for the task

$$e_{max} = \frac{\max_{t\in[0,T]} |F_M(t) - F_d(t)|}{\max_{t\in[0,T]} F_d(t)} \tag{15}$$

measures the worst instantaneous match. Finally, the total error

$$e_{tot} = \left|\int_0^T \left(F_M(t) - F_d(t)\right) dt\right| \tag{16}$$

captures how much the impulse delivered over the entire task differs from the target. In a freely moving constant-load system, e_{tot} is proportional to the velocity error at the end of the task, and, unlike e_{rms}, it does not penalise a muscle for compensation, that is, for force below the target during one part of the task but exceeding the target during another part.

Results

The muscle forces produced by all MU pools match the elementary tasks well after the neural drive has been optimised for these tasks (Figure 4). In general, the best and worse performing pools varied from task to task, although there is a slight tendency for the exponential-linear type MU pools to underperform in terms of e_{rms} and e_{max}. Compared to variations among MU pool types, the effects of varying the r_{max} scheme were even more task dependent, with no clearly favourable scheme emerging overall. The main variation between the pools arise from differences in peak F_d matching, which mainly affects e_{rms}. Additionally, the pools exhibit small variations in the timing of the ascending and descending edges of the produced force pulses, which particularly affects e_{max}.

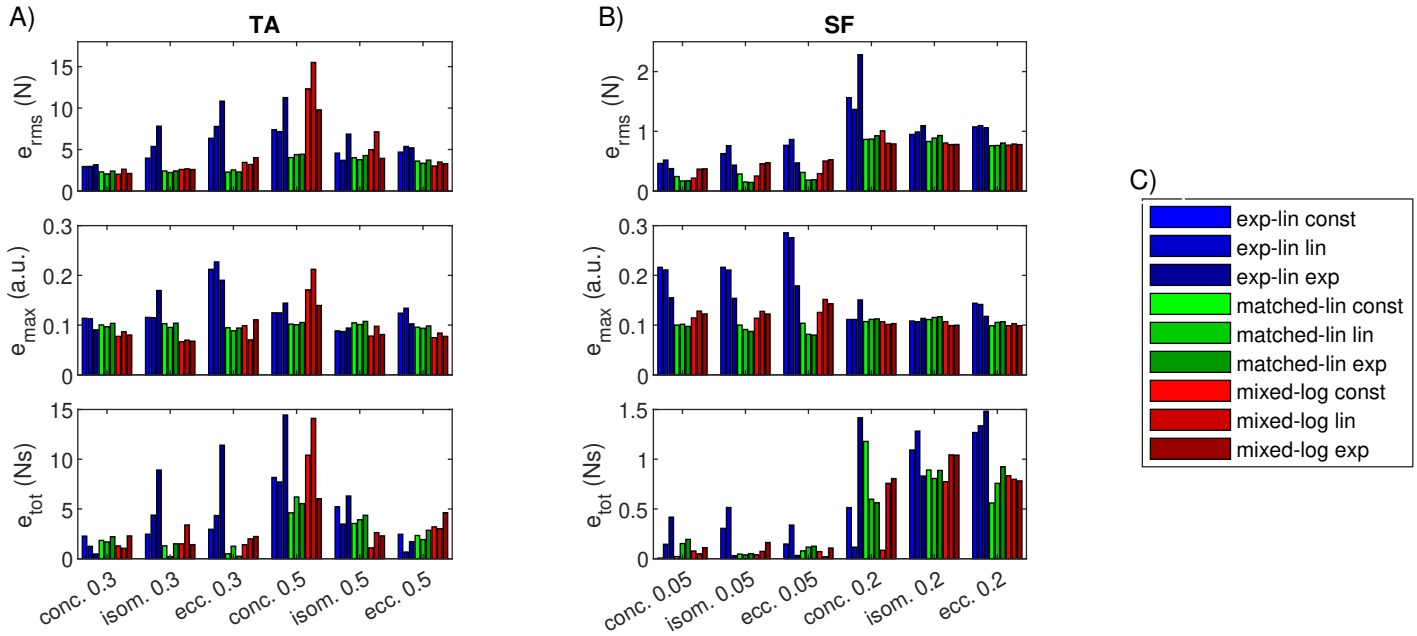

Fig 4. Force matching errors on scaled elementary tasks after optimisation. (A) Errors for the tibialis anterior MU pools for concentric, isometric, and eccentric tasks with force amplitudes $0.3F_{max}$ and $0.5F_{max}$. (B) Errors for the shoulder flexor MU pools for concentric, isometric, and eccentric tasks with force amplitudes $0.05F_{max}$ and $0.2F_{max}$. (C) Legend for the MU pool colours in panels A and B.

When used to represent the TA, all MU pools were able to match the trapezoidal target forces generally well (Fig 5). However, there are distinct differences in how accurately the plateau force is matched and more minor differences during the ascending and descending force ramps. The matched-linear type pools match the desired force profile the best when performance is measured using e_{rms} and e_{max} (Fig 6A), with the matched-linear pool with constant r_{max} producing the best matching

overall. The plateau force for all of the matched-linear pools was, on average, within 2.3 N of the target on both trapezoidal tasks. The exponential-linear pools and the mixed-logarithmic pools produced more varied results, with mixed-logarithmic pools generally performing better than exponential-linear pools at the lower force task while the different error measures favoured different pools at the higher force task. In terms of plateau force match, the exponential-linear pools produced sustained contraction, on average, at 4.9-12.4 N below the lower 120 N target and at 6.3-18.7 N above the higher 200 N target. The effect was opposite for the mixed-logarithmic pools, which produce 3.9-5.2 N in excess of the lower target and 7.7-18.4 N below the higher target. It is also worth noting that the exponential-linear pools display larger force variability during the plateau compared to the other models, although this variability is not unreasonable compared to human performance (see [2]).

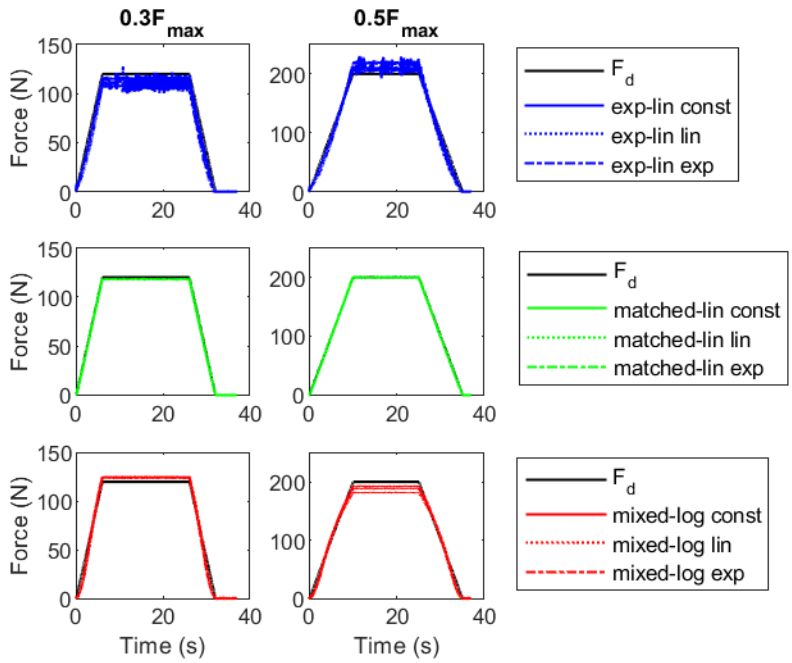

Fig 5. Force match for the trapezoidal tasks by TA. Panel columns show the two trapezoidal tasks. The force curves have been grouped by basic MU pool type.

No r_{max} scheme appeared to universally improve the ability of all MU pools to match the trapezoidal forces. However, exponentially decreasing r_{max} consistently led to worse performance in the exponential-linear MU pool model, and linearly decreasing r_{max} also caused the matched-linear pools to perform slightly worse. More prominently, the r_{max} scheme affects the firing rate patterns observed in the MUs during the task, as shown in Fig 7A for the $0.3F_{max}$ task (see S1 Fig for the higher force task), which displays the true instantaneous firing frequencies extracted from the excitation signals u_i and smoothed using a 5-sample moving average filter. There are two main differences in the firing rate behaviors of the MU pools. First, firing rates in the exponential-linear pools increase and decrease slowly during force ramping, whereas MUs in the other pools achieve their steady state firing rates nearly instantaneously. Qualitative comparison with firing rates extracted from high-density surface EMG data [2] during the same task (Fig 7B for three examples, see S2 Fig for full dataset) suggests that the slower rate increase matches real MU behaviour better, although some MUs, particularly those recruited late in the task, develop their maximum firing rates very

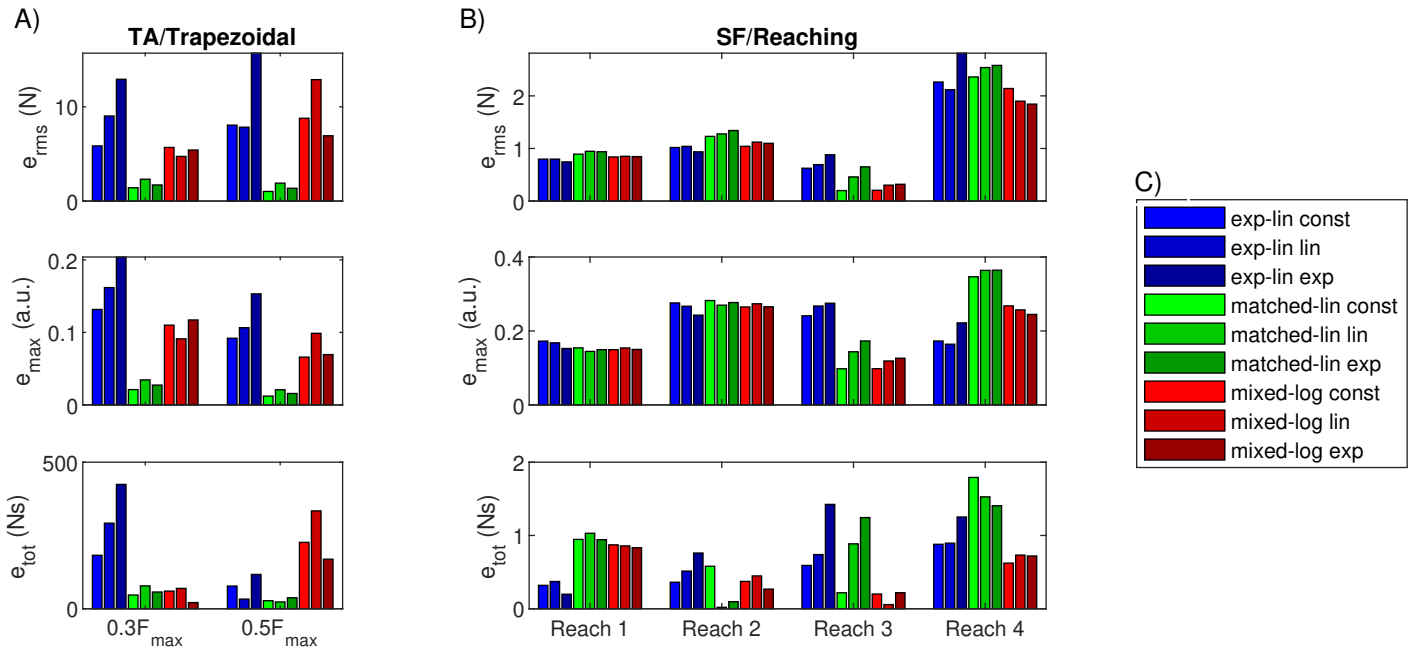

Fig 6. Force match errors in trapezoidal and reaching tasks (A) Performance of the nine MU pool models of the TA in two trapezoidal tasks. (B) Performance of the nine MU pool models of the SF in four reaching tasks. (C) Legend for the MU pool colours in panels A and B.

fast. Second, the range of maximum firing rates developed during the task vary by both MU pool type and by r_{max} scheme. While the variation in the maximum firing rate in the matched-linear pools can be attributed nearly solely to the r_{max} scheme, in the other pool types, MUs recruited later in the task can exhibit lower firing rates both due to decreasing $r_{max,i}$ and due to submaximal recruitment (i.e. $r_i < r_{max,i}$). The experimental data suggest that differences in the maximum firing rate of MUs and the pattern of lower firing rates in later recruited MUs are common but not always present in real muscle contractions.

Qualitative inspection of the experimental firing rate data from [2] also suggested that for some, but not all, test subjects, the $0.5F_{max}$ task elicited higher firing rates in the early recruited MUs than the $0.3F_{max}$ task (see S2 Fig). This behaviour cannot be replicated by the matched-linear and mixed-logarithmic pools without significant adjustment to the pool parameters; due to small recruitment bandwidths in these pool models, the firing rate of the smallest MUs reaches $r_{max,i}$ at low levels of desired force. In contrast, all of the exponential-linear pools show an increase in the firing frequencies of the smallest MUs as force demand is increased from $0.3F_{max}$ to $0.5F_{max}$. Hence, the nine pools presently studied fall grossly within the large range of behaviours exhibited by real muscles. However, the qualitative comparison suggests that the exponential-linear models produce firing rate patterns closest and the matched-linear models furthest from real muscle recruitment behaviour.

The performance of the MU pool models in representing a SF in the four reaching force matching tasks is shown in Fig 8 with corresponding error metrics displayed in Fig 6B. The overall error levels suggest that the mixed-logarithmic type MU pools tend to perform better than the other types of MU pools thanks to consistent behaviour across all four reaches, although the results are more varied when looking at e_{tot} for individual tasks. As with the TA and trapezoidal tasks, the r_{max} scheme has little

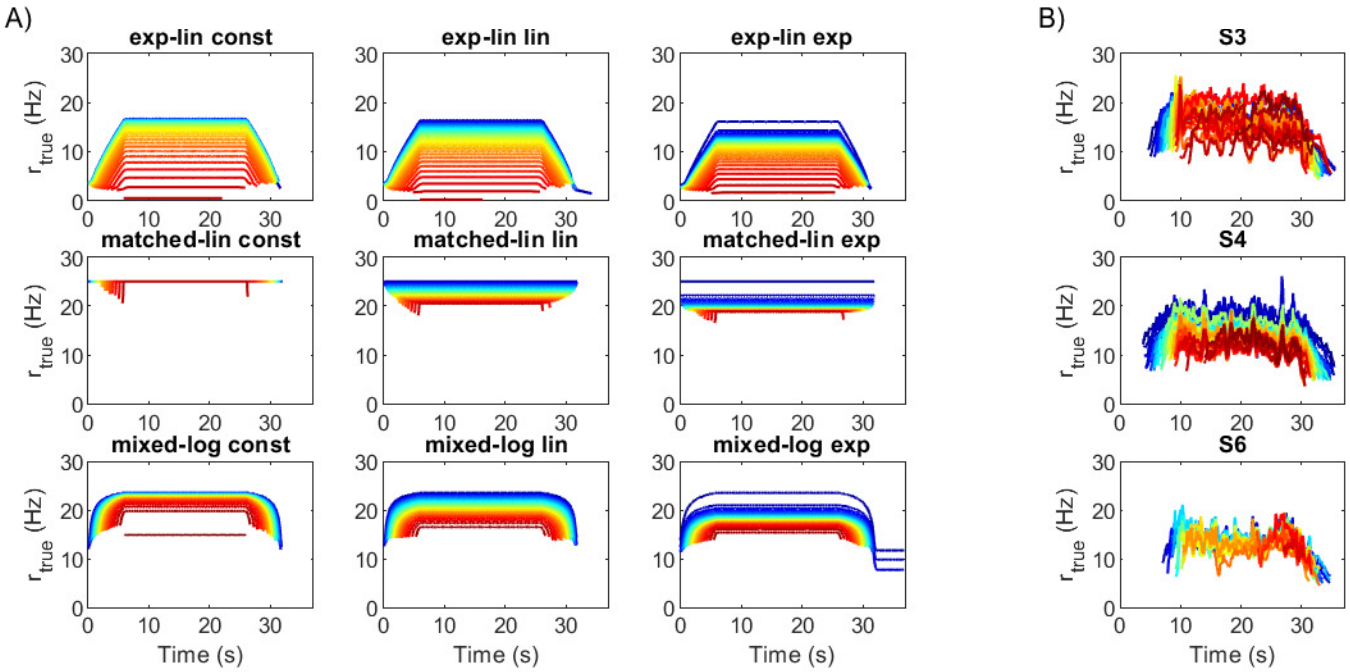

Fig 7. True firing frequencies for the TA/trapezoidal 0.3F_{max} task. (A) Simulated frequencies extracted from excitation impulse trains for the nine MU pools. (B) Examples (subjects S3, S4 and S6) of experimental data for the same task [2]. The colours in all panels indicate order of MU recruitment from first (dark blue) to last (dark red). Only every 10th MU is shown in A. Note that there is no correspondence between the ordering of panels in A and B.

impact on the overall performance, although it can affect the performance of each MU pool type in a task-dependent manner.

Inspection of the time signals (Fig 8) suggests that last two reaching tasks elicited the most variable performance from the MU pools. The MU pool models struggle to match both the low peak force and the even lower sustained contraction of reach 3, likely at least partially due to the relatively small number of MUs recruited. While the exact number of MUs active during reach 3 varies by pool, for comparison, the peak force corresponds roughly to the maximal contraction of the smallest 15 MUs in the pool and the sustained force to the smallest 3 MUs. In reach 4, the peak amplitude is less problematic, although not quite matched by the exponential-linear or the mixed-logarithmic pools. However, the rapid force decay followed by a second force peak in reach 4 proved difficult for the MU pools to match, with none of the pools reaching the desired local force minimum. Reaches 1 and 2 also have local force minima followed by secondary peaks, which the pools match largely successfully, so the problematic feature in reach 4 likely relates to the short time scale and timing of the force changes relative to the immediate history of MU firing.

Discussion

The present work aimed to determine how MU pool structure and recruitment strategy affect the fidelity of force matching for various mechanical tasks. Towards this goal, we simulated the performance of nine different MU pool models in two different cases: when they are used to represent a TA and match an isometric trapezoidal force profile, and when they are used to represent a SF and match simulated reaching force profiles while undergoing predetermined length and contraction speed changes. In general, our

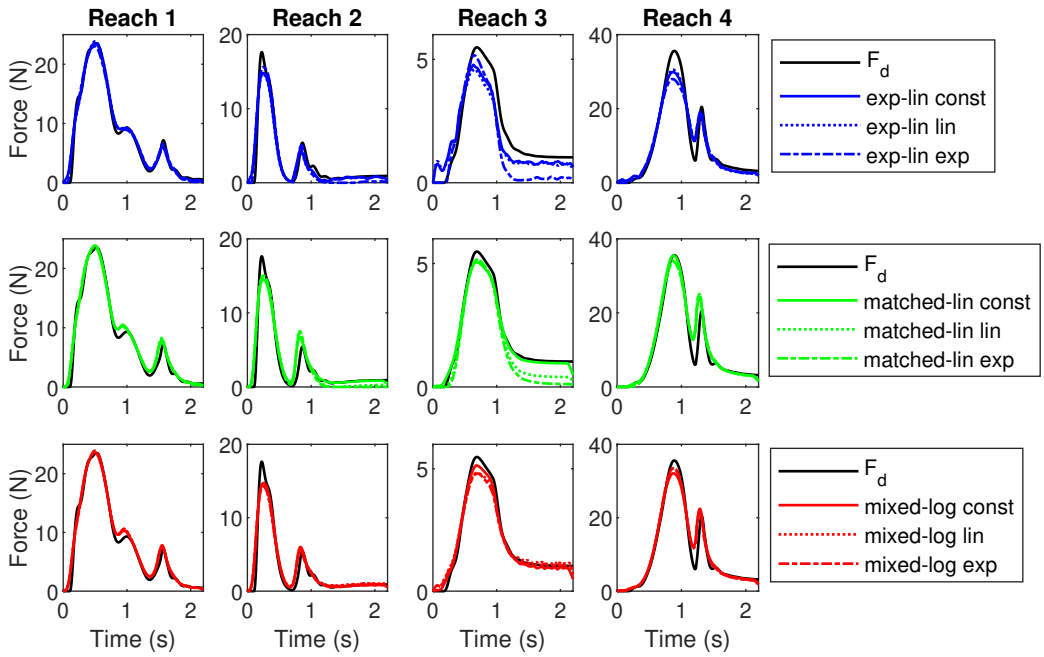

Fig 8. Force match for the simulated reaching tasks by SF. Panel columns show the four reaching tasks. The force curves have been grouped by basic MU pool type.

simulations using a neural drive mapping and sequential MU recruitment produced force patterns which closely matched desired force profiles. These force matches arose from direct simulation of physiological phenomena (rather than curve fitting), providing evidence that this approach can be useful for future forward dynamics studies of neuromuscular control.

Our simulation results suggest that the structure and characteristics of MU pools, represented by the different models, can impact the pools' ability to match a given force profile, but the differences are relatively small. We make five observations, in particular. 1) Relatively good force matches were obtained using a pure feedforward configuration, relying on a simple mapping from desired force to neural drive to govern MU recruitment and rate coding. 2) Enforcing onion-skin type behaviour through lower r_{max} of larger MUs had negligible impact on a MU pool's overall force matching accuracy across the tasks studied. 3) Of the MU pools studied, matched-linear models perform best for slowly varying or sustained isometric contractions for tasks of different force amplitudes. 4) The firing rate behaviour of exponential-linear pools during trapezoidal tasks exhibited the best qualitative match with experimental data. 5) Mixed-logarithmic pools performed most consistently well across a range of non-isometric reaching tasks.

The different MU pools were parameterised to match the first and last recruitment thresholds across the models. While this ensures comparability of the range of thresholds, it can also disadvantage certain pool structures. For example, the thresholds used to represent the TA forced most of the MUs in exponential-linear pools to operate at firing rates well below their r_{max} values during the trapezoidal tasks, leading to larger force fluctuations than in models where most recruited MUs reach r_{max}. Furthermore, while the case-study approach taken ensures that MU pool representations of the two different muscles are assessed on functionally relevant tasks, it also limits our ability to do strict cross-comparison between muscles and tasks. Hence, even where

simulation results disfavour a pool model, this does not preclude the possibility that a different parameterisation of the pool might decrease or eliminate the difference in performance. Given our goal of laying the foundations for using multi-MU muscles in MSK modelling, our results highlight the need to consider MU pool parameterisation as a whole from the perspective of functionality. While parameterisation based on experimental data is always desirable, it is not always feasible; factors such as differences between muscles [23, 26], individual variation (e.g. [25]), and task-dependent behaviour [26] of MUs pose challenges on combining data from different experiments.

Another feature of the present investigation which might lead to unequal treatment of different MU pools is the mapping from desired force to neural drive. Although the form of Eq (7)) is appealing because of the minimal number of parameters, it only allows for a limited manipulation of the desired force and FVL signals to obtain the neural drive. While this avoids overfitting the simulation dynamics to the specific demands of the elementary tasks, it can also favour MU pools whose steady-state neural drive to muscle force mapping is more linear. As the matched-linear pools have been artificially constructed to produce linear steady-state input-output behaviour, it is not surprising that they perform better than the other pool models in the trapezoidal tasks requiring slowly varying and sustained force production. Some of the disadvantage for the other pool models could be mitigated by obtaining multiple neural drive mappings focusing on narrower force ranges or by explicitly mapping and inverting the steady-state nonlinearity (as done in [19]). It is worth noting, however, that the matched-linear pools do not appear to have an advantage in reaching tasks, where the transient response of the MU pool dominates due to dynamically changing force demands.

True MU behaviour is complex, and for the MU pool models studied, some known effects had to be omitted. Motor neuron firing is a stochastic process, and most MU pool models include noise in the timing of the excitation impulses following [10]. Motor signal noise was left out of the present study to simplify parameter optimisation and comparison of force matching results in tasks where force demand changes rapidly and small differences in the timing of individual impulses can lead to large changes in output. The investigated MU pools also treat recruitment and derecruitment identically, whereas current-voltage hysteresis exhibited by real motor neurons leads to different thresholds and firing rates when muscle force generation is increasing and decreasing [28, 29]. While these effects can be incorporated by utilising different motor neuron properties during the descending phase of trapezoidal tasks (as done by, e.g., [3]), it is less clear how practicable this approach is for force profiles with multiple inflection points, such as our reaching tasks, especially as repeated activation can affect the hysteresis observed [29]. The effects of including these and other MU characteristics, such as fatigue and other time-dependent changes in MU behaviour (see e.g. [14–16] for models including them), are left for future studies.

In the present study, force matching has been looked at in isolation from its natural dynamic context. This approach enabled comparing different MU pools under strictly comparable non-isometric conditions. However, until future studies embed MU pool models in a forward dynamics MSK model, the significance of the force matching errors is difficult to evaluate. In a full forward dynamics model, the effects of a force mismatch could be partially mitigated by the intrinsic stabilising properties of muscle FVL characteristics [30–32]. Furthermore, the presence of redundant and antagonistic muscles would reduce the demand on an individual muscle to produce the desired force. Rather, the focus of the task would shift to coordinating the recruitment of multiple muscles to match desired joint torque, which might allow individual MU pools to find favourable operating points. Since the observed force matching errors were relatively small, a low level of feedback added to the presented feedforward control configuration might be able to correct it successfully. However, the responsiveness of a MU pool is

inherently limited by intrinsic factors such as the activation (and deactivation) dynamics of muscle fibres and the refractory period of motor neurons, placing constraints on changes in force production regardless of dynamic context. Hence, incorporating MU pool models in forward dynamics simulations is the next step towards understanding the extent to which inherent MU pool characteristics affect movement functionality.

In conclusion, our investigation signals that muscles consisting of multiple rate-coded MUs can match forces from various mechanical tasks, building the foundation for incorporating these models in MSK modelling. These MU pool models offer a significant advance over the non-physiological amplitude-coded single-MU muscle models in terms their realism, and they also open a range of new research questions and topics for investigation, such as the correspondence between the natural diversity in MU numbers and pool characteristics [23] and differences in function across muscles. Using traditional approaches, evaluation of the functional differences among the muscles with diverse MU populations would not be feasible.

Supporting information

S1 Fig. Firing frequencies for the TA/trapezoidal 0.5F_max task extracted from the excitation impulse trains for the nine MU pool models. The colours in all panels indicate order of MU recruitment from first (dark blue) to last (dark red). Only every 10th MU is shown.

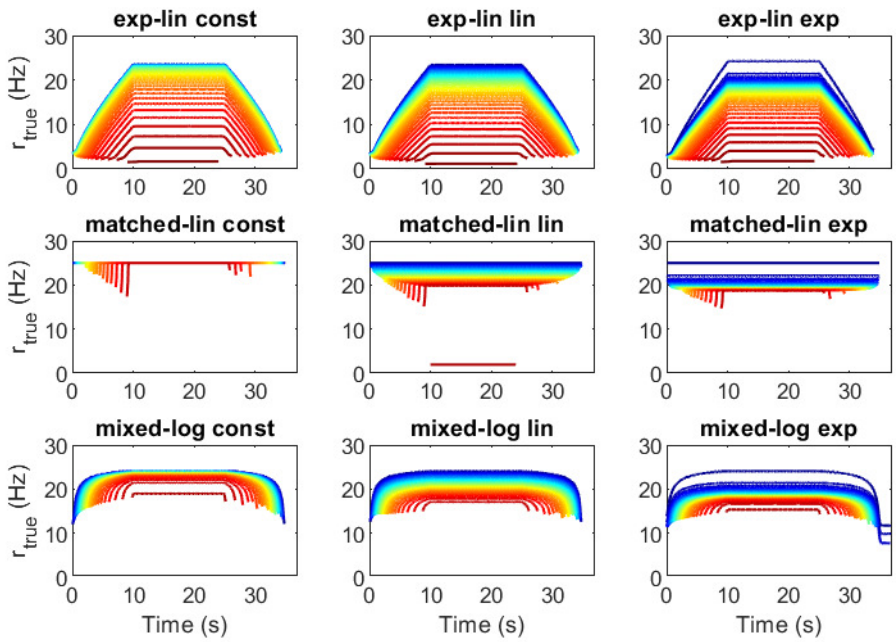

Fig 9. Supplementary Figure S1 Fig.

S2 Fig. Experimental firing frequencies during trapezoidal task. Data on firing instants from [2] is converted into firing rate curves by computing inter-impulse distances and using a moving average filter. Both $0.3F_{max}$ (left column) and $0.5F_{max}$ (right column) tasks are shown for six subjects (S1-S6), except the higher force task for subject S2, which was not included in the original dataset.

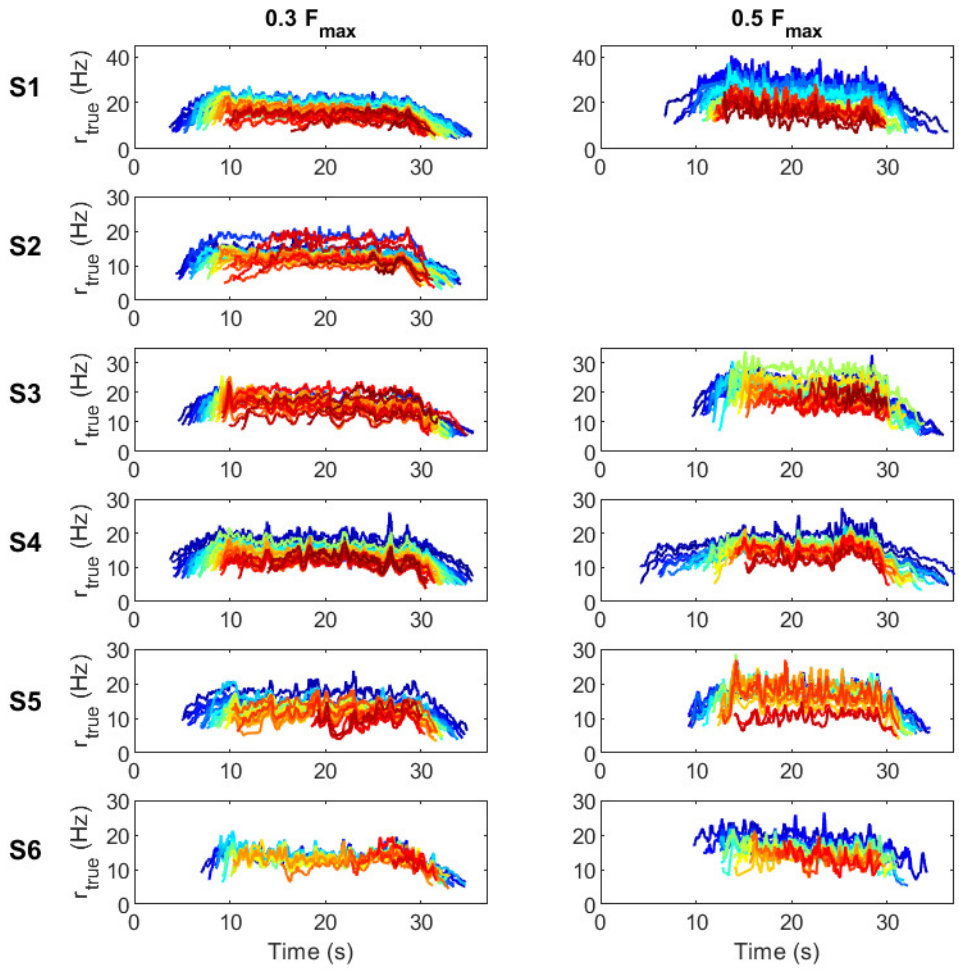

Fig 10. Supplementary Figure S2 Fig.

References

1. Hodson-Tole EF, Wakeling JM. Motor unit recruitment for dynamic tasks: current understanding and future directions. Journal of Comparative Physiology B. 2009;179:57–66.

2. Caillet AH, Avrillon S, Kundu A, Yu T, Phillips ATM, Modenese L, et al. Larger and Denser: An Optimal Design for Surface Grids of EMG Electrodes to Identify Greater and More Representative Samples of Motor Units. eNeuro. 2023;10(9). doi:10.1523/ENEURO.0064-23.2023.

3. Caillet AH, Phillips AT, Farina D, Modenese L. Estimation of the firing behaviour of a complete motoneuron pool by combining electromyography signal decomposition and realistic motoneuron modelling. PLOS Computational Biology. 2022;18(9):e1010556.

4. Del Vecchio A, Negro F, Holobar A, Casolo A, Folland JP, Felici F, et al. You are as fast as your motor neurons: speed of recruitment and maximal discharge of motor neurons determine the maximal rate of force development in humans. The Journal of physiology. 2019;597(9):2445–2456.

5. Thelen DG. Adjustment of muscle mechanics model parameters to simulate dynamic contractions in older adults. Journal Biomechanical Engineering. 2003;125(1):70–77. doi:10.1115/1.1531112.

6. Ong CF, Geijtenbeek T, Hicks JL, Delp SL. Predicting gait adaptations due to ankle plantarflexor muscle weakness and contracture using physics-based musculoskeletal simulations. PLoS computational biology. 2019;15(10):e1006993.

7. Delp SL, Anderson FC, Arnold AS, Loan P, Habib A, John CT, et al. OpenSim: open-source software to create and analyze dynamic simulations of movement. IEEE Transactions on Biomedical Engineering. 2007;54(11):1940–1950.

8. Kargo WJ, Rome LC. Functional morphology of proximal hindlimb muscles in the frog Rana pipiens. Journal of Experimental Biology. 2002;205(14):1987–2004.

9. Rajagopal A, Dembia CL, DeMers MS, Delp DD, Hicks JL, Delp SL. Full-body musculoskeletal model for muscle-driven simulation of human gait. IEEE Transactions on Biomedical Engineering. 2016;63(10):2068–2079.

10. Fuglevand AJ, Winter DA, Patla AE. Models of recruitment and rate coding organization in motor-unit pools. Journal of Neurophysiology. 1993;70(6):2470–2488.

11. Hu X, Rymer WZ, Suresh NL. Motor unit firing rate patterns during voluntary muscle force generation: a simulation study. Journal of neural engineering. 2014;11(2):026015.

12. Barry BK, Pascoe MA, Jesunathadas M, Enoka RM. Rate coding is compressed but variability is unaltered for motor units in a hand muscle of old adults. Journal of Neurophysiology. 2007;97(5):3206–3218. doi:10.1152/jn.01280.2006.

13. Nagamori A, Laine CM, Loeb GE, Valero-Cuevas FJ. Force variability is mostly not motor noise: Theoretical implications for motor control. PLoS Computational Biology. 2021;17(3):e1008707.

14. Dideriksen JL, Farina D, Baekgaard M, Enoka RM. An integrative model of motor unit activity during sustained submaximal contractions. Journal of Applied Physiology. 2010;108(6):1550–1562.

15. Dideriksen JL, Farina D, Enoka RM. Influence of fatigue on the simulated relation between the amplitude of the surface electromyogram and muscle force. Philosophical Transactions of the Royal Society A: Mathematical, Physical and Engineering Sciences. 2010;368(1920):2765–2781.

16. Potvin JR, Fuglevand AJ. A motor unit-based model of muscle fatigue. PLoS computational biology. 2017;13(6):e1005581.

17. Callahan DM, Umberger BR, Kent-Braun JA. A computational model of torque generation: neural, contractile, metabolic and musculoskeletal components. PloS one. 2013;8(2):e56013.

18. Henneman E. The size-principle: a deterministic output emerges from a set of probabilistic connections. Journal of experimental biology. 1985;115(1):105–112.

19. Petersen E, Rostalski P. A comprehensive mathematical model of motor unit pool organization, surface electromyography, and force generation. Frontiers in physiology. 2019;10:176.

20. Lai AK, Biewener AA, Wakeling JM. Metabolic cost underlies task-dependent variations in motor unit recruitment. Journal of the Royal Society Interface. 2018;15(148):20180541.

21. Contessa P, Luca CJD. Neural control of muscle force: indications from a simulation model. Journal of Neurophysiology. 2013;109(6):1548–1570.

22. Murtola T, Richards C. The impact of age-related increase in passive muscle stiffness on simulated reaching accuracy. Royal Society Open Science. 2023;10(2):221453.

23. Duchateau J, Enoka RM. Distribution of motor unit properties across human muscles. Journal of Applied Physiology. 2022;132(1):1–13.

24. Lee SSM, de Boef Miara M, Arnold AS, Biewener AA, Wakeling JM. EMG analysis tuned for determining the timing and level of activation in different motor units. Journal of Electromyography and Kinesiology. 2011;21(4):557–565. doi:10.1016/j.jelekin.2011.04.003.

25. De Luca C, LeFever R, McCue M, Xenakis A. Behaviour of human motor units in different muscles during linearly varying contractions. The Journal of physiology. 1982;329(1):113–128.

26. Enoka RM, Fuglevand AJ. Motor unit physiology: some unresolved issues. Muscle & Nerve: Official Journal of the American Association of Electrodiagnostic Medicine. 2001;24(1):4–17.

27. Flash T, Hogan N. The coordination of arm movements: an experimentally confirmed mathematical model. Journal of Neuroscience. 1985;5(7):1688–1703. doi:10.1523/JNEUROSCI.05-07-01688.1985.

28. Heckman C, Enoka RM. Motor unit. Comprehensive physiology. 2012;2:2629–2682.

29. Binder MD, Powers RK, Heckman C. Nonlinear input-output functions of motoneurons. Physiology. 2020;35(1):31–39.

30. van Soest AJ, Bobbert MF. The contribution of muscle properties in the control of explosive movements. Biological Cybernetics. 1993;69(3):195–204.

31. van der Burg J, Casius L, Kingma I, van Dieën JH, van Soest AJ. Factors underlying the perturbation resistance of the trunk in the first part of a lifting movement. Biological Cybernetics. 2005;93(1):54–62.

32. Haeufle D, Grimmer S, Seyfarth A. The role of intrinsic muscle properties for stable hopping—stability is achieved by the force–velocity relation. Bioinspiration & Biomimetics. 2010;5(1):016004.